A&A 556, A48 (2013)
DOI: 10.1051/0004-6361/201321773

Astronomy & Astrophysics

Reddening behaviors of young stellar objects in *Spitzer*/IRAC bands *(Research Note)*

Chae Kyung Sim[1], Sungsoo S. Kim[1,2], Jeong-Eun Lee[1,2], and Sang Joon Kim[1,2]

[1] School of Space Research, Kyung Hee University, Yongin, Gyeonggi 446-701, Korea
e-mail: cksim@khu.ac.kr
[2] Dept. of Astronomy & Space Science, Kyung Hee University, Yongin, Gyeonggi 446-701, Korea

Received 26 April 2013 / Accepted 11 June 2013

ABSTRACT

We investigate the reddening behaviors of young stellar objects (YSOs) in the photometric system of the InfraRed Array Camera (IRAC) onboard the *Spitzer* Space Telescope. We constructed a couple of model extinction laws for the IRAC wavelength range that are composed of a power-law function and a 9.7 μm absorption bump by silicates. We then calculated reddened colors of the YSOs in 3 different evolutionary stages with various masses and disk inclinations by convolving the adopted model spectral energy distributions (SEDs) with the spectral response functions of the IRAC bands for K_S-band extinction values of up to 8 mag. We find that the reddening vectors of YSOs in the [3.6]−[4.5] vs. [5.8]−[8.0] diagrams are considerably SED-dependent and can be highly nonlinear in some cases. Many YSOs show a "bluening" (as opposed to the reddening) in the [5.8]−[8.0] color owing to the 9.7 μm bump in the extinction law. Our findings imply that dereddening in a color–color or color–magnitude diagram involving the [8.0] band might be highly unreliable unless the SED of the source and the extinction law are at least approximately known.

Key words. dust, extinction – infrared: ISM – stars: formation – techniques: photometric

1. Introduction

Spitzer Space Telescope has been a great tool for detecting and studying deeply embedded young stellar objects (YSOs) and protostars in the near- and mid-infrared wavelength ranges. Photometry at [3.6], [4.5], [5.8], and [8.0] μm bands of the InfraRed Array Camera (IRAC), sometimes together with near-infrared J, H, and K bands and/or [24] μm band of the Multiband Imaging Photometer for *Spitzer* (MIPS), is widely used to identify YSOs and to study their properties (e.g., Allen et al. 2004; Robitaille et al. 2006; Gutermuth et al. 2008; Megeath et al. 2012). Color–color (CC) diagrams in the IRAC bands, the [3.6]−[4.5] vs. [5.8]−[8.0] diagram in particular, are useful for revealing the evolutionary stages and disk properties of the YSOs. For example, objects with accreting disks, objects with infalling envelopes, and objects without near-infrared excesses (including foreground/background stars) are relatively well segregated and separated from each other in the [3.6]−[4.5] vs. [5.8]−[8.0] diagram (Allen et al. 2004). For this reason, we concentrate on the reddening behaviors of YSOs in this CC diagram in the present study.

Photometry of the YSOs suffers extinction not only from interstellar medium but also from dense molecular clouds in which the YSOs are embedded. The amount of extinction differs even in the same molecular cloud and sometimes reaches as high as $A_K \sim 8$ mag (Cambrésy et al. 2011). Extinction correction is therefore a crucial step in estimating the intrinsic magnitudes and colors of the YSOs.

However, as shown by Kim et al. (2005, 2006) and Kim & Lee (2007), the reddening behavior of an object in the color–magnitude (CM) and CC diagrams is dependent on the spectral energy distribution (SED) of the object. Furthermore, the reddening vector can even be curved when the amount of extinction is significant. In this Note, we report the same reddening characteristics (SED dependence and nonlinearity of the reddening vectors) of YSOs in the IRAC bands.

We construct simple models for the extinction law in the IRAC bands in Sect. 2, and calculate the shifts of the effective wavelengths in Sect. 3. We then analyze the reddening behaviors in IRAC CC diagrams in Sect. 4 and summarize our work in Sect. 5.

2. Models

2.1. Model SEDs for YSOs

To study the extinction behavior of YSOs at various evolutionary stages, stellar masses, and disk inclinations, we have adopted the model SEDs by Robitaille et al. (2006). These models cover a variety of parameters including stellar masses from 0.1 to 50 $M_\odot$, evolutionary stages from the early envelope infall stage to the late disk-only stage, and inclinations from 18° (pole-on) to 87° (edge-on).

The classification scheme of YSOs suggested by Lada (1987) and improved by subsequent authors (Wilking et al. 1989; André et al. 1993; Greene et al. 1994) uses the spectral index α (the slope of $\log \lambda F_\lambda$ to $\log \lambda$) of the SED between 2- and 20 μm as an indicator. This system divides YSOs into four "classes": envelope-collapsing sources ($0.3 \geq \alpha$; Class I), flat spectrum sources ($-0.3 \leq \alpha < 0.3$; Flat), disk sources ($-1.6 \leq \alpha < -0.3$; Class II), and disk-dissipated sources ($\alpha < -1.6$; Class III). This spectral index indicator, however, is sometimes insufficient to directly relate the class to the actual evolutionary stage of the object.

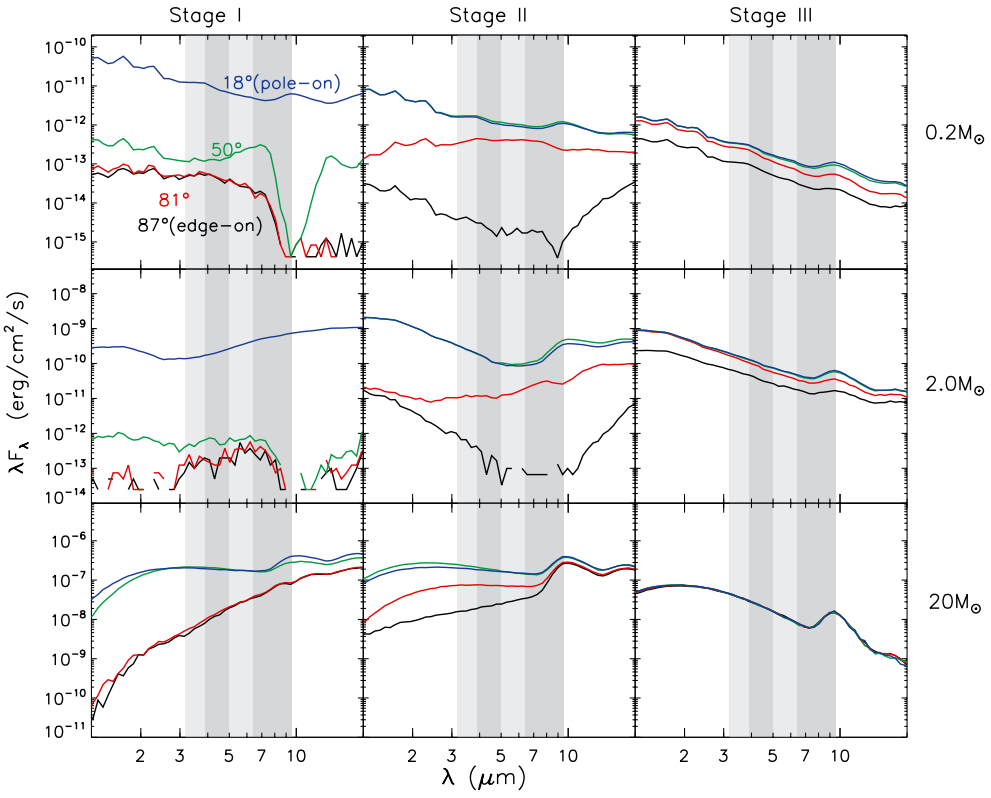

Fig. 1. Model SEDs of YSOs for Stages I, II, and III (from *left to right columns*), stellar masses of 0.2, 2.0, and 20 $M_\odot$ (from *top to bottom rows*), and for disk inclinations of 18.2° (blue, pole-on), 49.5° (green), 81.4° (red), and 87.1° (edge-on, black). Wavelength ranges of the four IRAC filters are marked with different tones of shades. We consider these 36 models in our analyses among 200 000 models provided by Robitaille et al. (2006).

Robitaille et al. (2006) show that the disk geometry also contributes significantly to the SED and changes the spectral index, particularly in the earlier stages where the infalling envelope obscures the central source. For this reason, instead of the spectral index indicator, they adopted the "stage" classification to refer the evolutionary stage of YSOs based on its envelope accretion rate ($\dot{M}_{\rm env}$) or disk mass ($M_{\rm disk}$) as follows: objects with significant infalling envelopes and possibly disks ($\dot{M}_{\rm env}/M_* > 10^{-6}$ yr^{-1}; Stage I), objects that have optically thick disks ($\dot{M}_{\rm env}/M_* < 10^{-6}$ yr^{-1} and $M_{\rm disk}/M_* > 10^{-6}$; Stage II), and objects that have optically thin disks ($\dot{M}_{\rm env}/M_* < 10^{-6}$ yr^{-1} and $M_{\rm disk}/M_* < 10^{-6}$; Stage III).

Robitaille et al. (2006) provide 200 000 SED models for random but physically meaningful combinations of various values of 12 parameters, including the stellar mass, the envelope accretion rate and radius, and the disk accretion rate and radii at ten viewing angles (disk inclinations). For our analyses in this Note, we chose the models that have the closest stellar mass to 0.2, 2.0, and 20.0 $M_\odot$ for each of three stages and four different disk inclinations (18.2°, 48.5°, 81.4°, and 87.1°[1]). The adopted model SEDs are shown in Fig. 1. We note that the 36 chosen models are just a few samples of a variety of SEDs provided by Robitaille et al. (2006) and that models with similar stellar masses can have quite different SEDs if they have considerably different values for other parameters for the envelope, disk, and cavity.

2.2. Extinction law in the IRAC wavelength regime

A single power-law function ($A_\lambda \propto \lambda^{-\beta}$) with an exponent β of 1.6–1.8 has been widely used as an extinction law for the wavelength range covered by J, H, and K bands (~1–~2.5 μm). At the wavelength range covered by the IRAC bands (~3–~10 μm), shallower extinction laws (smaller β) have been obtained from various observations (Lutz et al. 1996; Indebetouw et al. 2005; Flaherty et al. 2007; Nishiyama et al. 2009, among others). Furthermore, the 9.7 μm absorption feature by silicates can play an important role in the extinction at the IRAC wavelength regime (Indebetouw et al. 2005; Zasowski et al. 2009).

The exact extinction law in the IRAC bands is still quite uncertain, and finding or improving the extinction law in the IRAC bands is not within the scope of the present study. Instead, we model the extinction law as simply as possible with known observational and theoretical features and use it to find the characteristic reddening behaviors of YSOs in the IRAC CC diagrams.

Our model extinction law for the IRAC bands regime is composed of a single power-law function and a log-normal bump centered at 9.66 μm, the latter of which is for the absorption feature by astronomical silicates. Together with the extinction law in the near-infrared, our model can be written as

$$A_\lambda/A_{K_{\rm S}} = \begin{cases} (\lambda/2.14)^{-\beta_{JHK}} \\ (2.5/2.14)^{-\beta_{JHK}} \left\{ (\lambda/2.5)^{-\beta_{\rm IRAC}} + c_1 e^{-[c_2 \log(\lambda/9.66)]^2} \right\} \end{cases} \quad (1)$$

where the wavelength λ is in units of μm. We adopt $\beta_{JHK} = 1.7$ for the slope in the near-infrared following Rieke & Lebofsky (1985).

We obtain the IRAC regime slope $\beta_{\rm IRAC} = 0.68$ by fitting observed $A_{3.6}/A_{K_{\rm S}}$, $A_{4.5}/A_{K_{\rm S}}$, and $A_{5.8}/A_{K_{\rm S}}$ values, and determine the amplitude and width of the bump, c_1 and c_2, by fitting the observed $A_{8.0}/A_{K_{\rm S}}$ value. For observed $A_{\rm IRAC}/A_{K_{\rm S}}$ values, we considered the observations toward five star-forming regions by Flaherty et al. (2007, the Ophiuchus, Orion A, Serpens, NGC 2024/23, and NGC 2068/71) and one field in the Galactic plane by Indebetouw et al. (2005, $l = 284°$ region near the RCW 49), and adopted $A_{\rm IRAC}/A_{K_{\rm S}}$ values toward the Ophiuchus

[1] We chose these four inclinations because these values yield reasonably different SED shapes from each other.

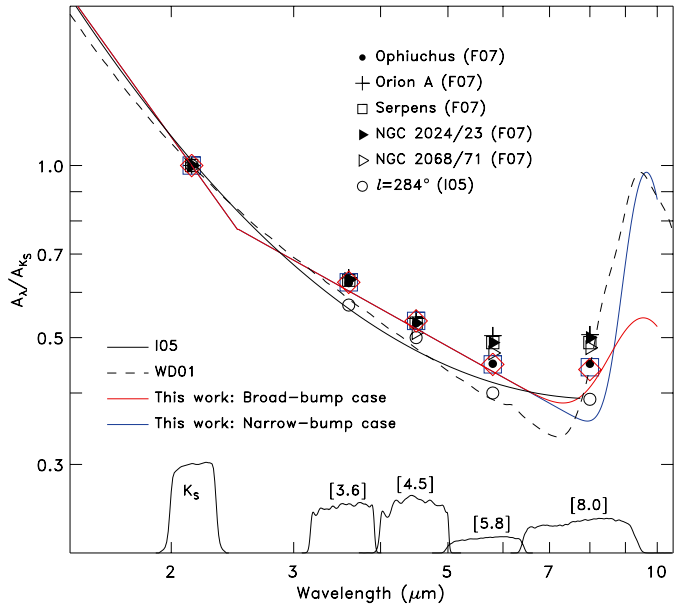

Fig. 2. Our extinction laws for the broad-bump (red line) and the narrow-bump cases (blue line), along with the extinction law of Weingartner & Draine (2001) and Indebetouw et al. (2005). Black symbols represent $A_{\rm IRAC}/A_{K_{\rm S}}$ values obtained by Flaherty et al. (2007) for five star-forming regions, the Ophiuchus, Orion A, Serpens, NGC 2024/23, and NGC 2068/71, and by Indebetouw et al. (2005) for a field (l = 284°) near the star-forming region RCW 49. Color symbols are the $A_{\rm IRAC}/A_{K_{\rm S}}$ values from our synthetic photometry for the SED of a Stage II, 2 $M_\odot$ YSO with an inclination of 81.4° and $A_{K_{\rm S}}$ = 1 mag. Also shown are the spectral response functions of $K_{\rm S}$ and four IRAC bands in arbitrary units.

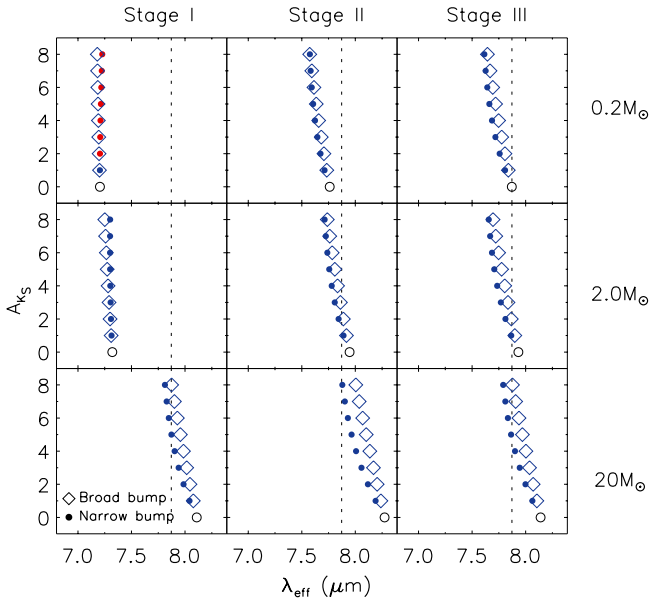

Fig. 3. [8.0]-band effective wavelengths ($\lambda_{\rm eff}$) of YSOs with an inclination of 81° for $A_{K_{\rm S}}$ values of up to 8 mag for the broad-bump (diamonds) and the narrow-bump cases (filled circles) of our extinction law. The reddened SEDs have been convolved with the IRAC [8.0] band response function to obtain the effective wavelengths. The effective wavelengths shifted redward from that at $A_{K_{\rm S}}$ = 0 (black open circles) are plotted in red and those shifted blueward are plotted in blue. The nominal wavelength of the IRAC [8.0] filter, 7.87 μm, is also shown with dashed lines.

because this region approximately gives the median $A_{\rm IRAC}/A_{K_{\rm S}}$ values of the above six regions. (We call these extinction ratios "the Ophiuchus extinction law"[2], hereafter.)

Since the width of the bump is not certain and may even vary from clouds to clouds (Chiar et al. 2007), we consider two different cases here, the broad and short bump (c_1 = 0.3, c_2 = 14.3) and the narrow and tall bump (c_1 = 0.86, c_2 = 26). In the broad-bump case, we adopted the c_2 value from the extinction law of Rosenthal et al. (2000) and obtained c_1 that fits the observed $A_{8.0}/A_{K_{\rm S}}$ value. In the narrow-bump case, we adopted the c_1 value from the case B, R_V = 5.5 extinction law of Weingartner & Draine (2001).

When fitting the $A_{\rm IRAC}/A_{K_{\rm S}}$ values, we convolved the SED of a Stage II YSO with a stellar mass of 2.0 $M_\odot$ and an inclination of 81° with the spectral response functions of the $K_{\rm S}$ (K-short) band[3] and the IRAC bands[4] for extinction of $A_{K_{\rm S}}$ = 1.

Our two model extinction laws are shown in Fig. 2 along with the convolved $A_{\rm IRAC}/A_{K_{\rm S}}$ values from our extinction laws and the observed $A_{\rm IRAC}/A_{K_{\rm S}}$ values by Indebetouw et al. (2005) and Flaherty et al. (2007). Figure 2 also shows model extinction laws suggested by Weingartner & Draine (2001) and Indebetouw et al. (2005) as comparisons.

[2] The Ophiuchus extinction ratios by Flaherty et al. (2007) are $A_{3.6}/A_{K_{\rm S}}$ = 0.623, $A_{4.5}/A_{K_{\rm S}}$ = 0.53, $A_{5.8}/A_{K_{\rm S}}$ = 0.45, and $A_{8.0}/A_{K_{\rm S}}$ = 0.45.

[3] http://www.ifa.hawaii.edu/instrumentation/quirc/quirc.html

[4] http://irsa.ipac.caltech.edu/data/SPITZER/docs/irac/calibrationfiles

3. Shift of the effective wavelength

As discussed in Sect. 1, Kim et al. (2005) and Kim & Lee (2007) showed that the reddening vectors in the near-infrared CM and CC diagrams can be noticeably nonlinear if the magnitude of the extinction is large enough, and they attributed this to the longward-shift (i.e., redshift) of the "effective wavelength" in a passband, which is caused by the wavelength-dependent extinction of the SED. The effective wavelength is defined by

$$\lambda_{\rm eff} = \frac{\int \lambda^2 f_\lambda S_\lambda {\rm d}\lambda}{\int \lambda f_\lambda S_\lambda {\rm d}\lambda}, \quad (2)$$

where f_λ is the *reddened* flux of the source, and S_λ the spectral response function of the passband.

We have examined the shifts of the effective wavelength in the IRAC photometry of YSOs for $A_{K_{\rm S}}$ values of up to 8 mag. While the effective wavelengths of the [3.6], [4.5], and [5.8] bands show redshifts as in the near-infrared bands, the effective wavelengths of [8.0] band shift *shortward* (i.e., blueshift) in most of the SEDs (see Fig. 3, which shows $\lambda_{\rm eff}$ values as a function of $A_{K_{\rm S}}$ for YSOs with an inclination of 81° as a sample). This unusual behavior is caused by the inversion of the extinction slope at 7.5–9 μm due to the 9.7 μm bump, so has not been seen in the optical or near-infrared passbands.

The $\lambda_{\rm eff}$ behavior as a function of extinction clearly shows an SED dependence, and this in turn results in the SED dependence of the reddening vectors in IRAC CC diagrams. The effects of the detailed SED shapes on the reddening behavior will be discussed in Sect. 4.

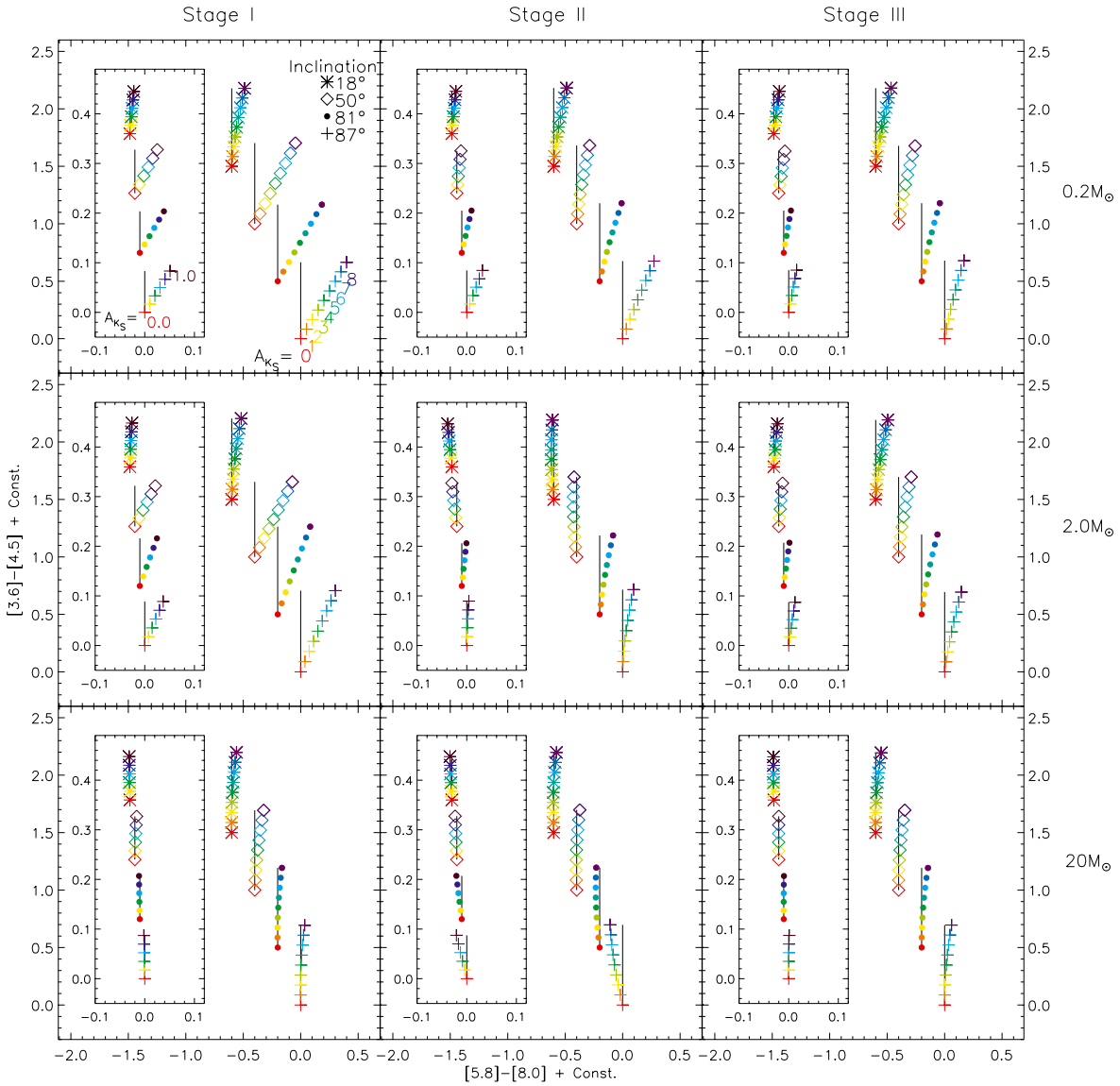

Fig. 4. IRAC color–color diagrams from our synthetic photometry for the 36 YSO SEDs at Stages I, II, and III (from *left to right columns*) with stellar masses of 0.2, 2.0, and 20 $M_{\odot}$ (from *top to bottom rows*), and disk inclinations of 18.2° (asterisks), 49.5° (diamonds), 81.4° (filled circles), and 87.1° (pluses). The SEDs are progressively reddened up to A_{K_S} = 8 mag using the broad-bump case of our extinction law. Color coding represents different A_{K_S} values (red for 0 mag). All [3.6]−[4.5] and [5.8]−[8.0] colors are relative to those for A_{K_S} = 0, and each sequence of reddening is shifted both vertically and horizontally for clear presentation. Insets show magnified CC diagrams for A_{K_S} of up to 1 mag. Vertical lines from A_{K_S} = 0 mag are also drawn as a guide for eyes.

4. SED dependence and nonlinearity of reddening vectors

We have calculated [3.6]−[4.5] and [5.8]−[8.0] colors for A_{K_S} values of up to 8 mag by convolving the 36 representative SEDs discussed in Sect. 2.1 with the four IRAC spectral response functions. Reddening vectors in [3.6]−[4.5] vs. [5.8]−[8.0] diagrams are presented in Fig. 4 (broad-bump case) and Fig. 5 (narrow-bump case).

These two figures show that the reddening vectors depend significantly on SED. In the broad-bump case, most of the reddening vectors are upright in the CC diagram, but some of them are inclined to the first quadrant. The upright angles occur because the amount of extinction in [5.8] and [8.0] bands is approximately the same due to the broad bump. However, some of the SEDs (e.g., Stage I, 0.2 $M_{\odot}$, inclination ≥50°) have sharp drops longward of ∼8 μm, and this greatly diminished the effect of the broad bump, resulting in non-negligible reddenings in [5.8]−[8.0] colors. This shows that the angle of the reddening vector in the IRAC CC diagram depends on the detailed SED shape.

In the narrow-bump case, the SED dependence of the reddening vector is also seen, but its nonlinearity is more important. Many of the reddening vectors are inclined to the second quadrant when the extinction is low (A_{K_S} < 2–3). This means that the [5.8]−[8.0] colors of these objects are "bluened", instead of reddened. This bluening is due to the rapid increase in the extinction at the red end of [8.0] band. Once the extinction reaches a certain threshold (A_{K_S} ∼ 2–3), however, the post-extinction SED in the narrow bump region becomes so negligible that only the power-law part of the extinction law determines the [5.8]−[8.0] color – now the extinction gives rise to reddening, as usual. The nonlinearity is important for the YSOs with steeply increasing SEDs in the [8.0] band, which are the cases with a bump near 8 μm in the

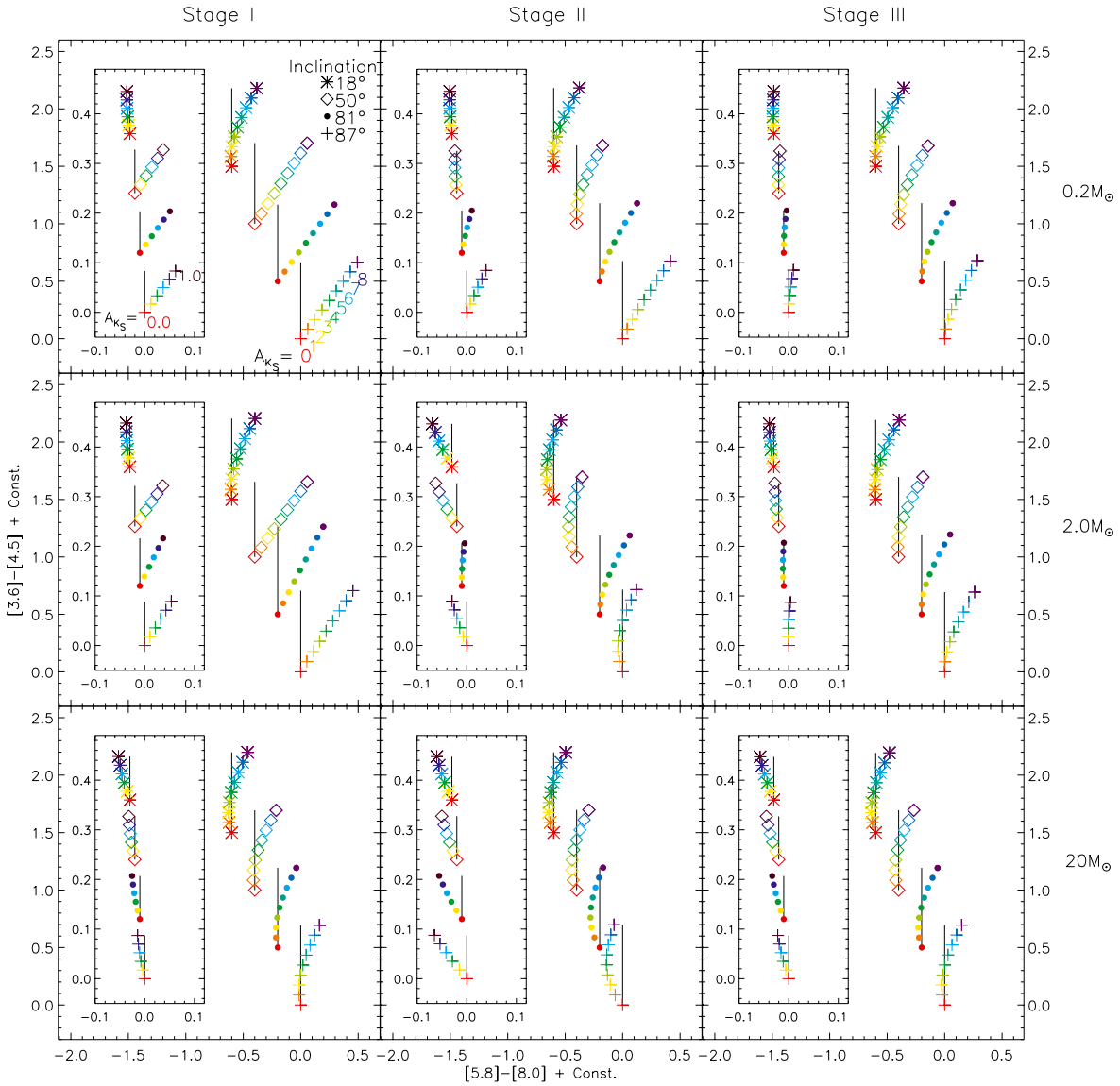

Fig. 5. Same as Fig. 4 but for the narrow-bump case of our extinction law.

SED. The nonlinearity is not significant for the SEDs that have a dropout at $\gtrsim$8 μm. For these SEDs, the effect of the narrow bump is negligible even for low extinctions.

The nonlinearity of the reddening vector, although small, is in fact seen in the broad-bump case as well. For example, the reddening vectors of Stage II YSOs with a stellar mass of 2.0 $M_\odot$ and inclinations of 81° and 87° are nearly upright when $A_{K_S} \lesssim 2$, but become moderately inclined to the first quadrant when the extinction is greater than ∼2. We note that for low extinctions ($A_{K_S} \lesssim 1$), the angle of the reddening vector is primarily determined by the presence of a dropout or a bump in the SED: the former tends to result in reddening vectors inclined to the first quadrant, and the latter to the second quadrant.

The extinction ratios derived from observations by Flaherty et al. (2007) are commonly used extinction laws for the IRAC bands, and the Ophiuchus extinction ratios mentioned in Sect. 2.2 are approximate averages of the six extinction ratios given in Flaherty et al. Figure 6 shows the offsets between the actual intrinsic colors and the dereddened colors when the Ophiuchus extinction ratios are used in dereddening the "observed" IRAC colors for A_{K_S} = 1, 4, and 8 mag. These offsets are not to be directly regarded as dereddening errors, because our extinction laws (Eq. (1)) are just models. The figure implies that the use of the same extinction ratios in dereddening various objects with different intrinsic colors (i.e., different SED shapes) is not appropriate particularly for [5.8]−[8.0] colors – it would tend to overestimate the intrinsic [5.8]−[8.0] colors for objects with intrinsically bluer [5.8]−[8.0] colors, and/or underestimate the intrinsic [5.8]−[8.0] colors for objects with intrinsically redder [5.8]−[8.0] colors.

Table 1 gives the minimum, median, and maximum offsets in the dereddened colors for A_{K_S} = 1, 4, and 8 mag among 80 284 samples that have disk inclinations of 18°, 50°, 81°, and 87° in the catalog of Robitaille et al. (2006). The span (max−min) in the offsets for A_{K_S} = 4 is only 0.15 mag for [3.6]−[4.5] color, but is 0.40 mag for the broad-bump case and 0.68 mag for the narrow-bump case. The latter values amount to 57% and 97% of the horizontal size of the Class II YSO area in the [3.6]−[4.5] vs. [5.8]−[8.0] diagram that is widely used in the studies of YSOs with IRAC photometries (central boxes in Fig. 6), implying that the possibility of misclassifying of YSOs due to inappropriate dereddening is not negligible for $A_{K_S} \gtrsim 4$.

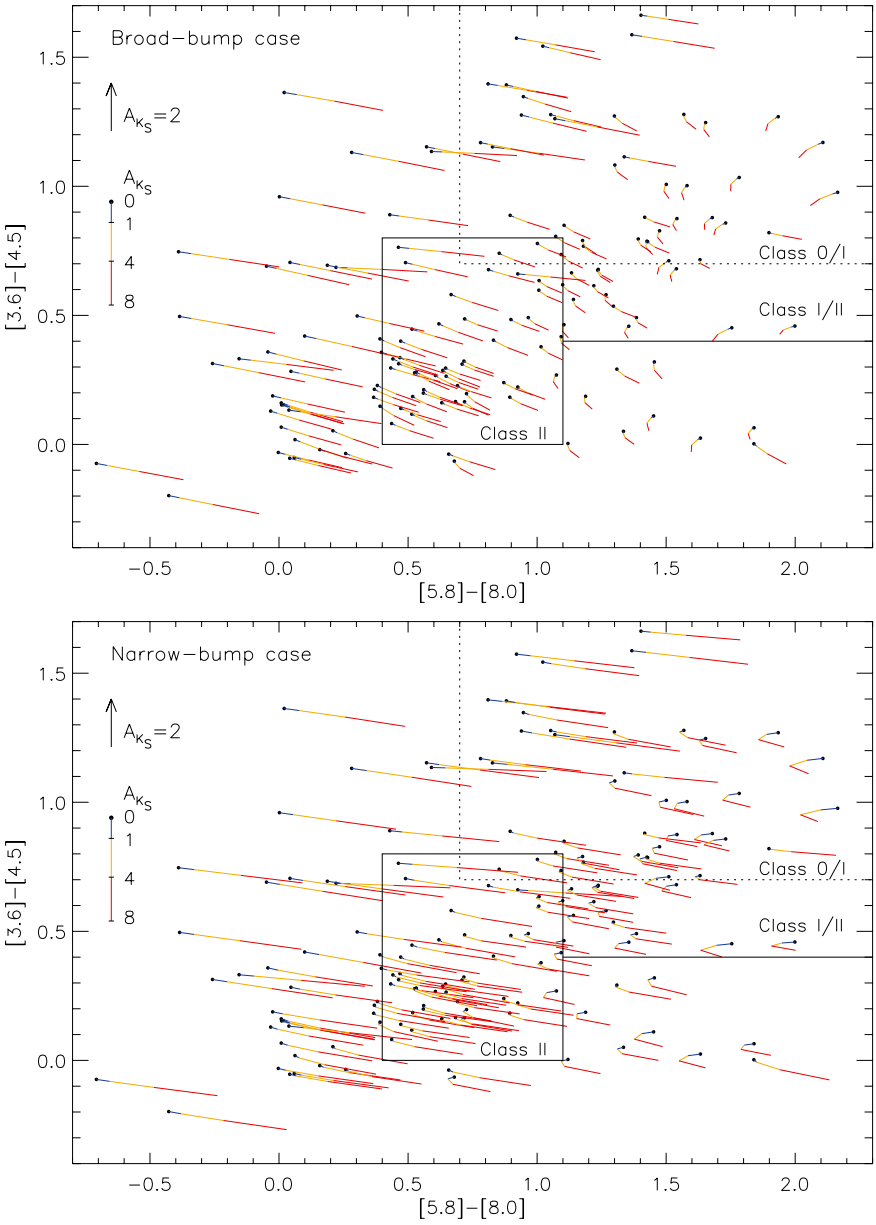

Fig. 6. Offsets of the dereddened colors from the actual intrinsic colors when the Ophiuchus extinction law (see Sect. 2.2) is used in dereddening the observed IRAC colors. The offsets are for 150 randomly chosen SEDs from 80 284 samples that have disk inclinations of 18°, 50°, 81°, and 87° in the catalog of Robitaille et al. (2006). The intrinsic colors are marked with black dots. We apply extinctions of A_{K_S} = 1, 4, and 8 mag to the chosen SEDs, calculate their synthetic IRAC magnitudes, then deredden the magnitudes using the Ophiuchus extinction ratios. Blue lines connect the intrinsic color and the simulated, dereddend color for A_{K_S} = 1 mag of each SED, yellow lines connect the dereddend colors for A_{K_S} = 1 and 4 mag, and red lines connect the dereddend colors for A_{K_S} = 4 and 8 mag. The arrows in the upper-left corners indicate the reddening vector for the Ophichus extinction ratios for A_{K_S} = 2 mag. The solid and dotted lines indicate the Class II, Class I/II, and Class 0/I areas in the IRAC CC diagram as suggested by Allen et al. (2004) and Samal et al. (2012).

5. Summary

We have investigated the reddening behaviors of YSOs in the *Spitzer*/IRAC bands. We constructed a couple of simple extinction laws for the mid-infrared wavelengths that are composed of a power-law function and a 9.7 μm bump. We calculated the reddening vectors in the IRAC CC diagrams for 36 YSO SEDs, and found that the reddening vectors are considerably SED-dependent and sometimes highly nonlinear. Our detailed findings can be itemized as follows:

1. Broad-bump case: The [5.8]−[8.0] color is a weak function of the extinction amount, resulting in relatively linear, upright reddening vectors in CC ([3.6]−[4.5] vs. [5.8]−[8.0]) diagrams.
2. Narrow-bump case: The reddening vectors in CC diagrams can be highly nonlinear for SEDs that increase steeply in the [8.0] band with increasing wavelengths.
3. Narrow-bump case: The [5.8]−[8.0] color can exhibit a "bluening" phenomenon when the extinction amount is less than 2–3 mag, resulting in reddening vectors inclined to the second quadrant in CC diagrams.
4. For SEDs with a dropout at $\gtrsim$8 μm, the reddening vectors are almost linear and inclined to the first quadrant of the CC diagram.
5. The use of the same extinction ratios in dereddening various objects with different SED shapes is not appropriate, particularly for [5.8]−[8.0] colors, and can result in an error in intrinsic [5.8]−[8.0] color that is as large as ~0.5 mag.

We conclude that dereddening in an IRAC color–color diagram involving the [8.0] band is highly unreliable unless the SED of the source and the extinction law are at least approximately known.

Acknowledgements. We thank Thomas Robitaille for generously giving us access to the full set of his SED models. This work was supported by the Mid-career Research Program (No. 2011-0016898) through the National Research Foundation (NRF) grant funded by the Ministry of Education, Science and Technology (MEST) of Korea. C.K.S. was supported by the WCU (World Class University) program through the NRF funded by the MEST (R31-10016).

Table 1. Offsets between the intrinsic colors and dereddened colors.

Color	A_{K_S}	(Dereddened color)−(Intrinsic color)			
		Minimum	Median	Maximum	Max−Min
	(mag)	(mag)	(mag)	(mag)	(mag)
		Broad-bump case			
[3.6]−[4.5]	1.0	−0.02	−0.01	0.02	0.04
	4.0	−0.09	−0.03	0.06	0.15
	8.0	−0.17	−0.05	0.13	0.30
[5.8]−[8.0]	1.0	−0.04	0.01	0.06	0.10
	4.0	−0.17	0.06	0.23	0.40
	1.0	−0.32	0.14	0.46	0.77
		Narrow-bump case			
[3.6]−[4.5]	1.0	−0.02	−0.01	0.02	0.04
	4.0	−0.09	−0.03	0.06	0.15
	8.0	−0.17	−0.05	0.13	0.30
[5.8]−[8.0]	1.0	−0.14	0.00	0.07	0.21
	4.0	−0.40	0.08	0.28	0.68
	8.0	−0.49	0.26	0.56	1.06

Notes. Dereddened colors are the colors that one would obtain by dereddening the observed IRAC colors using the Ophiuhus extinction law (see Sect. 2.2). The minimum, median, and maximum color offsets are for the 80 284 SED samples that have disk inclinations of 18°, 50°, 81°, and 87° in the catalog of Robitaille et al. (2006).

References

Allen, L. E., Calvet, N., D'Alessio, P., et al. 2004, ApJS, 154, 363
André, P., Ward-Thompson, D., & Barsony, M. 1993, ApJ, 406, 122
Cambrésy, L., Rho, J., Marshall, D. J., & Reach, W. T. 2011, A&A, 527, A141
Chiar, J. E., Ennico, K., Pendleton, Y. J., et al. 2007, ApJ, 666, L73
Flaherty, K. M., Pipher, J. L., Megeath, S. T., et al. 2007, ApJ, 663, 1069
Greene, T. P., Wilking, B. A., Andre, P., Young, E. T., & Lada, C. J. 1994, ApJ, 434, 614
Gutermuth, R. A., Myers, P. C., Megeath, S. T., et al. 2008, ApJ, 674, 336
Indebetouw, R., Mathis, J. S., Babler, B. L., et al. 2005, ApJ, 619, 931
Kim, S. S., & Lee, M. G. 2007, PASP, 119, 1449
Kim, S. S., Figer, D. F., Lee, M. G., & Oh, S. 2005, PASP, 117, 445
Kim, S. S., Figer, D. F., & Lee, M. G. 2006, PASP, 118, 62
Lada, C. J. 1987, in Star Forming Regions, eds. M. Peimbert, & J. Jugaku, IAU Symp., 115, 1
Lutz, D., Feuchtgruber, H., Genzel, R., et al. 1996, A&A, 315, L269
Megeath, S. T., Gutermuth, R., Muzerolle, J., et al. 2012, AJ, 144, 192
Nishiyama, S., Tamura, M., Hatano, H., et al. 2009, ApJ, 696, 1407
Rieke, G. H., & Lebofsky, M. J. 1985, ApJ, 288, 618
Robitaille, T. P., Whitney, B. A., Indebetouw, R., Wood, K., & Denzmore, P. 2006, ApJS, 167, 256
Rosenthal, D., Bertoldi, F., & Drapatz, S. 2000, A&A, 356, 705
Samal, M. R., Pandey, A. K., Ojha, D. K., et al. 2012, ApJ, 755, 20
Weingartner, J. C., & Draine, B. T. 2001, ApJ, 548, 296
Wilking, B. A., Lada, C. J., & Young, E. T. 1989, ApJ, 340, 823
Zasowski, G., Majewski, S. R., Indebetouw, R., et al. 2009, ApJ, 707, 510